Desalination and Water Treatment
www.deswater.com
doi: 10.5004/dwt.2023.29666

299 (2023) 179–189
July

Valorization of face mask waste as an adsorbent for cationic dye adsorption

Goy Khai Sze[a,†], Anis Atikah Ahmad[a,b,*], Azduwin Khasri[a,b]

[a]*Faculty of Chemical Engineering & Technology, Universiti Malaysia Perlis (UniMAP), Perlis, Malaysia, emails: anisatikah@unimap.edu.my (A.A. Ahmad), s181141467@studentmail.unimap.edu.my (G.K. Sze), azduwin@unimap.edu.my (A. Khasri)*
[b]*Centre of Excellence, Water Research and Environmental Sustainability Growth (WAREG), Universiti Malaysia Perlis (UniMAP), Perlis, Malaysia*

Received 27 October 2022; Accepted 7 June 2023

ABSTRACT

The increasing environmental pollution caused by the disposal of untreated dye-containing effluent and face mask wastes in landfills has become a significant concern. To address this issue, this work focuses on the utilization of face mask wastes as alternative adsorbents for the adsorption of malachite green (MG) dye. These adsorbents offer advantages such as ease of operation, cost-effectiveness, high efficiency, and ready availability. In this study, the raw face mask wastes (RFM) undergo a thermal treatment process in a furnace at 800°C for 21 h before conducting the adsorption tests. The Fourier-transform infrared spectroscopy analysis revealed the presence of various functional groups, including alkane, alkene, alcohol, and carbonyl, in both the treated face mask adsorbent (TFMA) and RFM. The scanning electron microscopy with energy-dispersive X-ray spectroscopy analysis displayed the surface morphologies of RFM as a porous and homogeneous carbon sorbent structure, while TFMA exhibited a heterogeneous and flaky structure. Energy-dispersive X-ray spectroscopy analysis indicated that RFM primarily consisted of carbon elements, followed by oxygen and calcium elements, whereas TFMA predominantly comprised calcium and oxygen elements with a limited amount of carbon. The adsorption experiments, considering various parameters such as initial dye concentration (1,000–1,200 mg/L) and contact time (5–1,500 min), demonstrated that increasing the contact time and initial concentration led to an enhanced adsorption capacity. The maximum adsorption capacity of 2,127 mg/g confirmed the effectiveness of TFMA as an adsorbent for MG. Thermodynamic analysis revealed that the adsorption process was spontaneous and endothermic. The isotherm and kinetic studies showed a good fit between the adsorption data and the Brunauer–Emmett–Teller and pseudo-second-order models as evidenced by high R^2 values and low error function values, suggesting a heterogenous adsorption of MG on TFMA.

Keywords: Face mask waste; Dye adsorption; Malachite green

1. Introduction

Coronavirus disease (COVID-19) that first detected on December 31, 2019 in Wuhan, China and continuously spread globally until today forced humans to wear a disposable face mask to protect against the spreading of this pandemic. The use of face masks has reduced the viral spread of COVID-19. However, there were approximately 129 billion face masks disposed to the environment globally every month [1]. A single N95 mask and a disposable surgical mask contains 11 and 4.5 g of polypropylene and other plastic derivatives such as polyethylene, polyurethane, polystyrene, polycarbonate and poly-acrylonitrile [2]. The discarded of single-use face masks under ambient

* Corresponding author.
† Co-authors.

conditions slowly degrade into smaller particles (<5 mm), which may form a new source of microplastics causing environmental pollution and threatening living organisms. Thus, effective plastic waste management, including reusing and recycling, is of great necessity.

The textile industry is a significant contributor to pollution, releasing highly concentrated effluents into the environment, thereby causing water pollution. This escalating water pollution has become a grave concern, posing a threat to the sustainability of various living organisms. Improper disposal of synthetic dyes into water bodies, such as rivers, without adequate treatment, leads to severe problems and raises serious concerns. With over 10,000 dyes being employed in industries like textiles, paper, cosmetics, and food, a substantial amount of dye-containing wastewater is generated. Several methods are available for the removal of dyes, including precipitation, coagulation, filtration, oxidation, and adsorption. Among these techniques, adsorption stands out as the most convenient, efficient, rapid, and cost-effective method for removing pollutants. Given the promising advantages it offers, adsorption has been widely adopted for the removal of pollutants.

In this study, face mask waste has been selected as the primary raw material for the development of an adsorbent. This choice is motivated by the increased demand for face masks during the ongoing global COVID-19 pandemic. The aim is to upcycle face mask waste into a high-value polypropylene (PP)-based adsorbent, which can then be utilized for effective dyes adsorption. This approach not only brings economic benefits to the waste management industry but also offers an environmentally friendly solution for wastewater treatment. The study focuses on utilizing face mask waste as a precursor to produce an adsorbent specifically designed for malachite green (MG) adsorption. Prior to the adsorption test, the face mask waste (RFM) undergoes a thermal treatment at a temperature of 800°C for a duration of 21 h. The characteristics of both the untreated and treated face mask adsorbents will be thoroughly analyzed to assess their potential as an effective MG adsorbent. The research will include a parametric study to examine the influence of initial dye concentration and contact time on MG adsorption. Additionally, isotherm and kinetic studies will be conducted to elucidate the mechanism of MG adsorption on the PP-based adsorbent, with the assistance of the MATLAB curve fitting tool.

2. Materials and methods

2.1. Materials

2.1.1. Precursor preparation and physical activation

The raw materials required for this study consisted of face masks obtained from a local shop, along with MG (HmbG Chemicals, Malaysia) and distilled water provided by the Bioprocess Laboratory School in Jejawi, Perlis, Malaysia.

In this study, a furnace was employed to produce the treated face mask adsorbents (TFMA) by exposing them to a temperature of 800°C for a period of 21 h. The purchased face mask samples were assumed to be virtually free of contaminants. Subsequently, the aluminum strip and rubber straps of the face masks were manually removed, and the face masks were manually cut to reduce their size, thereby increasing the surface area prior to the thermal treatment [3]. In the thermal treatment process, the remaining face mask material (RFM) was placed into a crucible and inserted into the furnace. The temperature was raised to 800°C, and the reaction was allowed to proceed for 21 h to ensure completion [4]. Once cooled, the resulting products, namely the treated face mask adsorbents (TFMA), were collected from the furnace. The weight of the RFM was measured before and after treatment using a weighing balance to determine the yield of the adsorbent.

2.1.2. Preparation of stock solution of malachite green

A stock solution of MG dye was prepared by adding 2 g of MG powder to distilled water, resulting in a total volume of 1 L and a concentration of 2 g/L [5]. This stock solution, containing the cationic dye ($C_{52}H_{54}N_4O_{12}$), was utilized as an adsorbate to assess the adsorption capacity of TFMA within a range of different concentrations, from 1,000 to 1,200 mg/L of MG [6]. To achieve these varied concentrations, the stock sample with a concentration of 2,000 mg/L was diluted using distilled water. The utilization of these high concentration ranges was intended to comprehensively assess the adsorption capacity of TFMA and explore any potential limitations.

In this research, the standard curve of the MG solution for 617 nm was prepared using the serial dilution method [7]. A stock solution of 2 g/L MG was utilized and subjected to a series of sequential dilutions. The resulting diluted solutions were then subjected to UV testing to obtain absorbance readings, which were used to construct the calibration graph.

2.2. Characterization methods

2.2.1. Fourier-transform infrared spectroscopy

The identification of functional group presents in RFM and TFMA was carried out using Fourier-transform infrared spectroscopy (FTIR) (PerkinElmer FTIR Spectrum 65). The FTIR analysis involved the preparation of a blank KBr disc and a sample KBr disc (containing RFM mixed with KBr powder). Both KBr discs were then transferred into a sample holder with a cap and subjected to scanning using FTIR spectrometry. The same procedure was repeated for testing TFMA. The resulting disc samples were placed in the instrument and scanned in the transmittance mode (%T) within the wavenumber range of 4,000–400 cm^{-1} at a resolution of 2 cm^{-1} [8].

2.2.2. Scanning electron microscopy with energy-dispersive X-ray spectroscopy

In this study, the surface structure, elemental identification, and qualitative compositional information of both RFM and TFMA were analyzed using scanning electron microscopy with energy-dispersive X-ray spectroscopy (SEM/EDX) (TM3000 Hitachi Tabletop Microscope). Magnifications ranging from x50 to x1,000 were utilized. The scanning electron microscopy (SEM) analysis involved

the evaluation of topography (surface features), morphology (particle shape and size), composition (elemental composition and relative amounts), and crystallographic information (atom arrangement) based on the obtained SEM micrographs. Additionally, the energy-dispersive X-ray spectroscopy (EDX) techniques were employed to provide chemical analysis of the observed features in SEM.

2.3. Adsorption test

2.3.1. Effect of initial concentration on MG adsorption capacity

The relationship between initial concentration and MG adsorption capacity was examined by manipulating a 100 mL MG sample in aqueous solution. The concentration of MG was varied at 1,000; 1,050; 1,100; 1,150 and 1,200 mg/L in the sample. Subsequently, the sample was transferred to separate 250 mL conical flasks for further analysis. Each conical flask was supplied with 0.05 g of TFMA and subjected to continuous stirring at 200 rpm for 1,500 min at 40°C [9]. To quantify the efficiency of MG dye removal, the percentage of dye removal was calculated using Eq. (1), which allowed for an evaluation of the adsorption capacity:

$$\text{Removal of MG dye}(\%) = \frac{C_i - C_F}{C_i} \times 100 \tag{1}$$

where C_i and C_F are the initial and final concentrations of MG (mg/L), respectively.

2.3.2. Effect of contact time on MG adsorption capacity

The effect of contact time on MG adsorption capacity was evaluated by manipulating the contact time of adsorption performance test with 5 min in each interval (5, 10, 15, 20, 25, 30, 60, 120, 180, 240, 360, 1,440 and 1,500 min) at 40°C [10]. This operation was performed at 200 rpm [9]. The conical flasks within the time interval were removed, filtered and the filtered solutions were tested using a UV spectrophotometer. The amount of MG dye adsorbed by TFMA at each time interval were then calculated by Eq. (2):

$$q_t = \frac{C_i - C_t}{M} \times V \tag{2}$$

where the C_i and C_t represented the initial concentration of MG dye solution and concentration of MG at the time, t while M represents the TFMA's weight (g) and V represent volume of MG dye solution utilized (L).

2.4. Adsorption isotherm analysis

The experimental data was fitted to the following isotherm and kinetic equations by employing MATLAB (R2020a) curve fitting tools software to solve for the unknown parameters by minimizing the error functions:

2.4.1. Langmuir adsorption isotherm

The Langmuir equation was displayed as non-linear form:

$$Q_e = \frac{Q_0 K_L C_e}{1 + K_L C_e} \tag{3}$$

where Q_e = the amount of adsorbate adsorbed at equilibrium (mg/g), C_e = the amount of adsorbate in the aqueous phase at equilibrium (mg/L), Q_0 = the theoretical maximum adsorption capacity (mg/g), K_L = the Langmuir constant (L/g).

2.4.2. Freundlich adsorption isotherm model

The Freundlich adsorption isotherm model derived a non-linear expression as:

$$Q_e = K_F C_e^{1/n} \tag{4}$$

where Q_e = adsorption capacity at equilibrium (mg/g), C_e = equilibrium concentration of adsorbate (mg/L), K_F = constant indicative of the relative adsorption capacity of the adsorbent, n = the degree of dependence of adsorption on the C_e of adsorbate.

2.4.3. Brunauer–Emmett–Teller adsorption isotherm model

The Brunauer–Emmett–Teller (BET) adsorption isotherm model derived a non-linear expression as:

$$Q_e = \frac{Q_{m,\text{BET}} K_S C_e}{\left(1 - K_L C_e\right)\left(1 + K_S C_e - K_L C_e\right)} \tag{5}$$

where Q_e = adsorption capacity at equilibrium (mg/g), C_e = equilibrium concentration of adsorbate (mg/L), K_L = equilibrium constant of adsorption for upper layers (L/mg), K_S = equilibrium constant of adsorption for first layer (L/mg), $Q_{m,\text{BET}}$ = amount of adsorbate corresponding to complete monolayer adsorption (mg/g).

2.4.4. Harkins–Jura adsorption isotherm model

The Harkins–Jura adsorption isotherm model derived a non-linear expression as:

$$Q_e = \left[\frac{B_{\text{HJ}}}{A_{\text{HJ}} - \ln\left(C_e / C_s\right)}\right]^{1/2} \tag{6}$$

where Q_e = adsorption capacity at equilibrium (mg/g), A_{HJ} = Harkins–Jura constant, B_{HJ} = Harkins–Jura constant, C_e = equilibrium concentration of adsorbate (mg/L), C_S = adsorbate monolayer saturation concentration (mg/L).

2.5. Adsorption kinetic analysis

2.5.1. Pseudo-first-order adsorption kinetic model

The pseudo-first-order model non-linear equation was then derived as:

$$q_t = q_e\left[1 - e^{-k_1 t}\right] \tag{7}$$

where q_t = absorbate adsorbed onto adsorbent at time t (mg/g), q_e = equilibrium adsorption capacity (mg/g), k_1 = equilibrium rate constant (L/min).

2.5.2. Pseudo-second-order kinetic adsorption model

The non-linear equation of the pseudo-second-order kinetic adsorption model was then derived as:

$$q_t = \frac{k_2 q_e^2 t}{1 + k_2 q_e t} \tag{8}$$

2.6. Thermodynamics study

Thermodynamic parameters of malachite green adsorption were studied by applying the Van't Hoff equation [11]. Experimental data obtained from adsorption test from various temperatures are employed to determine thermodynamic parameters such as Gibbs free energy change ($\Delta G°$), change in enthalpy ($\Delta H°$) and change in entropy ($\Delta S°$). The thermodynamic equilibrium constant (dimensionless) was approximated by the maximum adsorption capacity of adsorbate adsorbed (Q_{max}) and Langmuir constant (K_L) which is described in Eq. (9).

$$K_c = K_d = Q_{max} \times K_L \tag{9}$$

$$\ln K_c = -\frac{\Delta H}{RT} + \frac{\Delta S}{R} \tag{10}$$

$$\Delta G = -RT \ln K_c \tag{11}$$

where C_e is the concentration of sorbent at equilibrium condition, K_c is the constant at equilibrium and R is the natural gas constant.

3. Results and discussion

3.1. Characterization of RFM and TFMA

3.1.1. Fourier-transform infrared spectroscopy

RFM and TFMA were subjected to FTIR and the percentage transmissions for various wave numbers are displayed in Table 1 and Fig. 1. Table 1 demonstrates the presence of multiple distinct and well-defined absorption bands in RFM and TFMA. These include the peak at 2,918.85 cm^{-1} in RFM and 2,919 cm^{-1} in TFMA, which can be attributed to the stretching vibration of C–H resulting from the asymmetric and symmetric stretching vibrations of the alkene group (–CH_2). Additionally, the band at 2,952.44 cm^{-1} in RFM indicates the presence of the alkane group (–CH_3). The peak at 1,423.32 and 1,377.22 cm^{-1} in RFM, along with the peak at 1,428.92 cm^{-1} in TFMA, were identified as the results of the CH_3 group's asymmetric and symmetric deformation

Table 1
Functional groups in raw and treated face mask adsorbent

Group	Raw face mask adsorbent (RFM)			Treated face mask adsorbent (TFMA)		
	Wave number	Appearance	Functional group	Wave number	Appearance	Functional group
O–H stretching	–	–	–	3,644.80	Strong, broad	Alcohol
C–H stretching	2,952.44 2,918.85	Strong	Alkane Alkene	2,919	Strong	Alkene
C–H deformation	1,423.32 1,377.22	Weak, broad Strong	Alkane	1,428.92	Weak, Broad	Alkane
C–C stretching, CH_3 rocking, C–H wagging vibration	1,100.61	Medium	Glucose ring	1,099.4	Medium	Glucose ring
C–O stretching	875.22 713.44	Strong Strong	Carbonyl	876.27	Medium	Carbonyl

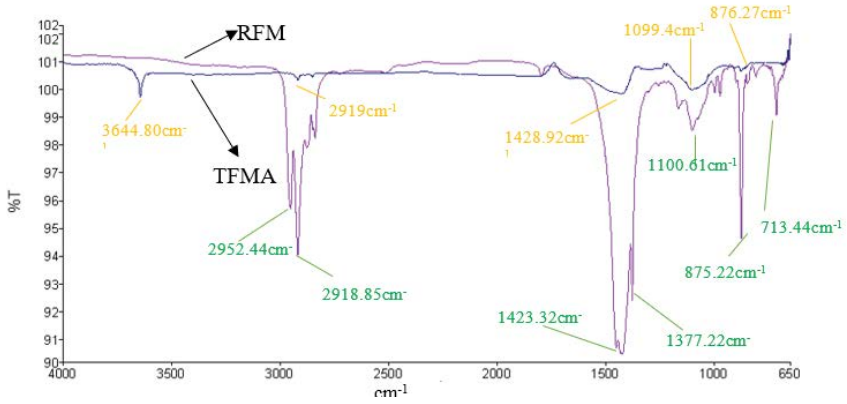

Fig. 1. Fourier-transform infrared spectra of RFM and TFMA.

vibrations. Meanwhile, the peak observed at 1,100.61 cm^{-1} in RFM, as well as 1,099.4 cm^{-1} in TFMA, indicates the presence of glucose rings stretching in the fiber, which correlates with C–C stretching, CH_2 rocking, and C–H wagging. The formation of the carbonyl group through C–O stretching of the face mask is attributed to the small peaks observed at 875.22 and 713.44 cm^{-1} in RFM, as well as 876.27 cm^{-1} in TFMA. Lastly, the peak observed at 3,644.80 cm^{-1} indicates the stretching of the O–H bond in the alcohol group of TFMA, serving as evidence for its presence.

By comparing the intensity of functional groups formed within RFM and TFMA, it was observed that some of them increased or decreased after undergoing thermal treatment. This change can be attributed to the thermal treatment, which provides sufficient energy for bond breaking of C–C and C–H bonds, leading to the formation of double bond groups such as the carbonyl group. The stretching vibration of functional groups observed in the FTIR spectra serves as evidence to prove that RFM and TFMA are polymeric materials that act as thermoplastics. Similar findings regarding the chemical characteristics of face masks have been reported by Aragaw [12] and Wang et al. [13] in their respective studies.

3.1.2. Scanning electron microscopy with energy-dispersive X-ray spectroscopy

Fig. 2 illustrates the surface morphological characteristics of the RFM and TFMA, which were analyzed using a SEM/EDX. The RFM, typically composed of a melt-blown material sandwiched between two layers of non-woven fabric, displayed a spherical porous structure that may enhance its adsorption performance. This finding aligns with a study conducted by Aragaw [12] who investigated disposable face masks as potential carriers of antibiotics in freshwater and seawater. Similarly, the surface morphologies of TFMA residues exhibited a heterogeneous, flaky structure, indicating successful thermal treatment.

Table 2 presents the elemental analysis of the RFM and TFMA. The analysis revealed that the RFM primarily consisted of carbon, followed by oxygen and calcium elements. In contrast, the TFMA was mainly composed of calcium and oxygen, with a limited amount of carbon. This difference can be attributed to the chemical reaction between carbon and oxygen during the thermal treatment of the RFM, resulting in the formation of carbon dioxide, which is then released into the surrounding environment [14]. Additionally, the heating process may lead to the formation of calcium-based compounds, such as calcium carbonate ($CaCO_3$), calcium peroxide (CaO_2), and calcium oxide (CaO), causing the formation of white ash powder instead of black biochar. By comparing the SEM photos and EDX results of RFM and TFMA, it can be concluded that the presence of calcium in the adsorbent alters its morphology and consequently enhances its adsorption performance [15].

3.2. Adsorption studies

3.2.1. Effect of contact time

Fig. 3 provides compelling evidence that the uptake of MG improves over time, eventually reaching a constant value, which indicates the saturation of TFMA's adsorption capacity. Initially, as the contact time increases, the adsorption capacity is enhanced, gradually leading to an equilibrium state. In the first 5 min, there is a significant and rapid increase in the adsorption capacity as the malachite green molecules are rapidly adsorbed onto the external surface of the treated face mask adsorbent (TFMA). As the process progresses, the rate of dye adsorption gradually slows down until it reaches the equilibrium point, indicating that the adsorbent has achieved its maximum adsorption capacity. The results of the adsorption study suggest that the time profile of MG dye uptake can be described as a single, smooth, and continuous curve, culminating in saturation.

Table 2
Elemental analysis of RFM and TFMA

Material	Composition (%)		
	C	Ca	O
RFM			
Inner	68.9	8.8	22.4
Middle	88.9	0.7	10.4
Outer	70.1	8.1	21.8
TFMA	7.3	46.5	46.2

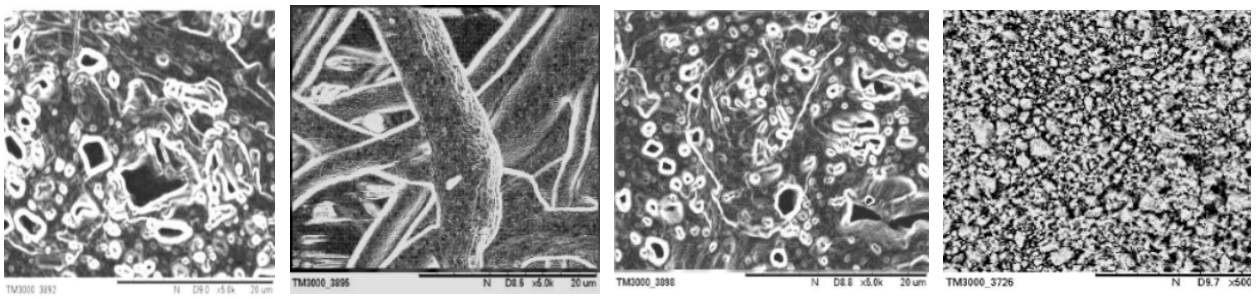

(a) (b)

Fig. 2. (a) Scanning electron microscopy photo of outer layer, middle layer and inner of RFM and (b) scanning electron microscopy photo of TFMA.

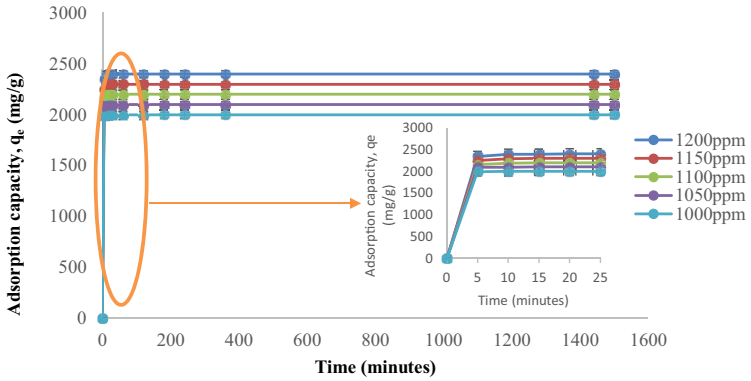

Fig. 3. Adsorption capacity of MG onto TFMA against time at different initial concentrations of dye.

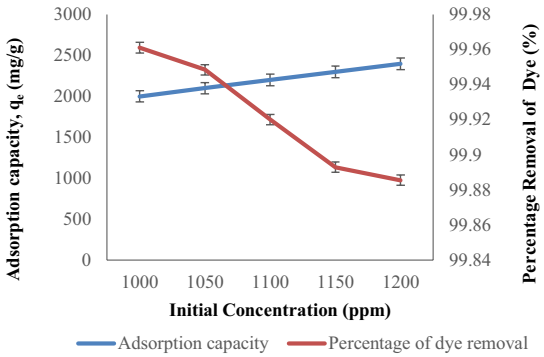

Fig. 4. Effect of initial concentration of MG on adsorption capacity of MG onto TFMA and its percentage of dye removal (0.5 g/L TFMA, 1,000–1,200 mg/L MG, 200 rpm).

This phenomenon supports the hypothesis that a monolayer coverage of dye forms on the surface of TFMA, as there are abundant available sites on the TFMA surface that can be occupied by MG particles during the initial stages of contact time [16]. Initially, the MG molecules rapidly attach to the exterior surface of TFMA at a high adsorption rate. However, as the adsorption of the exterior surface approaches saturation, the molecules begin to penetrate the pores of TFMA and adhere to its interior surface, which requires a relatively longer contact time. Consequently, as the contact time increases, it allows sufficient time for the MG molecules to occupy the available sites on TFMA, facilitating effective removal of the dye. This finding aligns with the study conducted by Nuradibah et al. [17] who investigated the adsorption of acrylic acid from wastewater using palm ash.

3.2.2. *Effect of initial concentration of MG (adsorbate)*

Fig. 4 provides valuable insights into the impact of initial concentration on the adsorption of MG onto TFMA. It is observed that as the initial concentration of dye increases, the percentage removal of dye experiences a drastic decline, while the adsorption capacity of MG onto TFMA increases [18,19]. The initial dye adsorption concentration plays a crucial role as the driving force in overcoming resistance encountered during the interaction between dye molecules in aqueous and solid phases [20,21]. Fig. 4 demonstrates

Table 3
Isotherm models fitting

Isotherm/constants/error function	Value
Langmuir isotherm	
Q_{max} (mg/g)	2,401
K_L (L/mg)	89.91
R^2	0.9976
RMSE	50.21
SSE	10,080
Freundlich isotherm	
n	11.46
K_F (L/g)	2,587
R^2	0.9997
RMSE	16.33
SSE	1,067
BET isotherm	
K_L (L/mg)	0.3182
K_S (L/mg)	246.1
$Q_{m,BET}$ (mg/g)	2,127
R^2	1.0000
RMSE	3.55
SSE	37.81
Harkins–Jura isotherm	
A_{HJ}	0.01449
B_{HJ}	2.719e+07
C_S (mg/L)	44.37
R^2	0.9999
RMSE	12.85
SSE	495.1

a clear increasing trend in the initial concentration of dye, ranging from 1,000 to 1,200 mg/L, which results in an increase in adsorption capacity from 1,999.2 to 2,397.25 mg/g. This can be attributed to the stronger mass transfer driving force present at higher initial concentrations. When the MG initial concentration is higher, the mass transfer rate is

Table 4
Adsorption kinetic model's parameter value for MG adsorption onto TFMA at various initial concentrations

Kinetic model	Parameter					
		Dye initial concentration (mg/L)				
		1,000	1,050	1,100	1,150	1,200
	$Q_{e,exp}$ (mg/g)	2,000.10	2,099.99	2,199.95	2,299.66	2,399.33
Pseudo-first-order	$Q_{e,calc}$ (mg/g)	1,999	2,099	2,189	2,297	2,386
	k_1 (min^{-1})	1.234	1.238	10.02	0.7672	9.629
Pseudo-second-order	$Q_{e,calc}$ (mg/g)	2,001	2,101	2,216	2,318	2,419
	k_2 (min^{-1})	0.02991	0.02801	0.00335	0.00287	0.00273

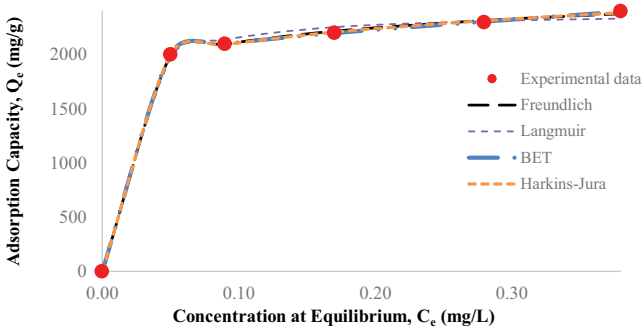

Fig. 5. Fitting of adsorption data with isotherm models.

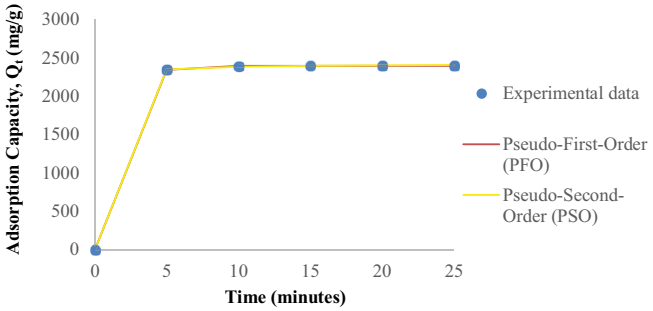

Fig. 6. Fitting of adsorption data with pseudo-first-order and pseudo-second-order.

driven by a larger concentration gradient between the MG in the liquid phase and TFMA in the solid phase, leading to a higher adsorption uptake of MG onto TFMA. A similar observation was made by Banerjee et al. [22] in their study on the adsorption of tartrazine onto activated carbon-based cola nut shells. In summary, Fig. 4 highlights the influence of initial concentration on the adsorption behavior of MG onto TFMA. Higher initial concentrations lead to an increased adsorption capacity but a decreased percentage of dye removal due to limitations in TFMA's adsorption sites.

3.3. Adsorption isotherm

The experimental data obtained from the MATLAB fitting tools revealed that the Langmuir and Freundlich isotherm models had R^2 values of 0.9976 and 0.9997, respectively. This indicates that the experimental data exhibited a better fit to the Freundlich model, suggesting the possibility of multilayer adsorption on the heterogeneous surface of MG adsorption onto TFMA. However, since the R^2 values for both Langmuir and Freundlich models were nearly identical, two additional multilayer isotherm models, namely BET and Harkins–Jura, were employed to fit the adsorption data of TFMA.

The Harkins–Jura model assumes the presence of a heterogeneous pore distribution and can be applied to multilayer adsorption, similar to the BET model. It was observed that the experimental data showed good fits to both the BET and Harkins–Jura models, with R^2 values of 1.000 and 0.9999, and root mean square error (RMSE) values of 3.55 and 12.85, respectively. Therefore, these results suggest that

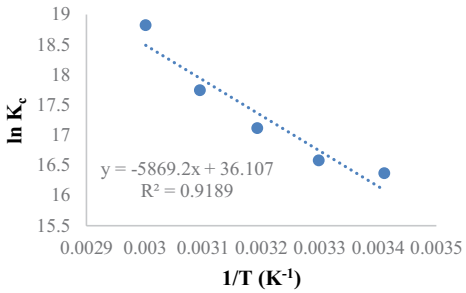

Fig. 7. Plot of lnK_c vs. T.

the adsorption of MG follows a multilayer adsorption mechanism over the heterogeneous surface of TFMA. Based on the evaluation of R^2, RMSE, and sum of squares of errors (SSE), the best-fitting models can be ranked in the following order: BET > Harkins–Jura > Freundlich > Langmuir.

The results obtained from the MATLAB fitting curve tools indicate that the BET model predicts a maximum monolayer saturation capacity of MG at 2,127 mg/L, which is slightly lower than the value predicted by the Langmuir model. The 1/n value predicted by the Freundlich model provides insights into the adsorption intensity of MG and the heterogeneity of the TFMA surface. The range of 0 to 1 for the 1/n value signifies favorable adsorption, with a lower value indicating a more heterogeneous adsorbent surface. In this case, the 1/n value of 0.087 suggests that the adsorption of MG onto the heterogeneous surface of TFMA is favorable.

Table 5
Kinetic error function data on adsorption of MG onto TFMA using non-linear regression analysis

Error function	Model	Initial concentration (mg/L)				
		1,000	1,050	1,100	1,150	1,200
R^2	Pseudo-first-order	1	1	0.9996	1	0.9995
	Pseudo-second-order	1	1	1	1	1
RMSE	Pseudo-first-order	1.202	1.472	19.06	3.529	23.42
	Pseudo-second-order	0.5003	0.7319	3.359	4.305	4.532
SSE	Pseudo-first-order	5.778	8.671	1453	49.81	2193
	Pseudo-second-order	1.001	2.142	45.13	74.13	82.17

3.4. Adsorption kinetic

Based on the analysis using MATLAB curve fitting tools, it can be observed that both the pseudo-first-order and pseudo-second-order models fit the experimental data well, as indicated by their high R^2 values close to or equal to 1, as shown in Table 5. However, the pseudo-second-order model was chosen as the preferred kinetic adsorption model for this research. This decision is based on the evaluation of parameters obtained from the MATLAB curve fitting tools, which demonstrate an overall higher R^2 value of 1 for the pseudo-second-order model, along with lower values of RMSE and SSE, as presented in Table 5. A lower RMSE value signifies a better fit and higher accuracy of the kinetic model in describing the adsorption behavior, while a lower SSE value indicates that the model fits well and is useful for prediction purposes. Furthermore, upon comparing the experimental value ($Q_{e,\exp}$) with the predicted value ($Q_{e,\text{calc}}$) obtained from the pseudo-first-order and pseudo-second-order models, it is evident that the values derived from the pseudo-second-order model are in closer agreement with the experimental data. This observation suggests that the adsorption process follows a second-order reaction, indicating a chemisorption mechanism where adsorption occurs through the sharing of electrons between the surface of the adsorbent and the adsorbate, leading to the formation of covalent or ionic bonds [23,24].

3.5. Adsorption thermodynamics

In Table 6 the negative values of $\Delta G°$ indicate that the adsorption process is spontaneous. Moreover, as the temperature increases, the $\Delta G°$ values also increase, suggesting that the adsorption process becomes more thermodynamically favorable at higher temperatures. This finding supports the idea that the adsorption of MG on TFMA is a favorable and spontaneous process.

The positive value of $\Delta S°$ indicates an increase in randomness and disorder at the solid/solution interface, highlighting the stable adsorption process of MG on TFMA. Additionally, the positive value of $\Delta H°$, with a relatively high adsorption enthalpy exceeding 40 kJ/mol, suggests that the adsorption is an endothermic process. This indicates the possibility of chemisorption, where chemical bonds are formed between MG and TFMA during the adsorption process. Similar observations have been reported by Gebreslassie [25] and Ahmad et al. [11] in their studies on malachite green adsorption using *Ficus cartia* leaves and gasified *Glyricidia sepium* woodchip, respectively.

Table 6
Thermodynamic parameters for adsorption of malachite green onto treated face mask adsorbent

Parameters	Temperature (K)	Results
$\Delta G°$ (kJ/mol)	293.15	–39.89
	303.15	–41.80
	313.15	–44.56
	323.15	–47.68
	333.15	–52.13
$\Delta H°$ (kJ/mol)		48.80
$\Delta S°$ (kJ/mol·K)		0.30

3.6. Application of treated face mask adsorbent as dye adsorbent

3.6.1. Comparison of TFMA with other adsorbents

The comparison of adsorption capacities between previous studies and the treated face mask waste adsorbent is presented in Table 7. The results indicate that TFMA exhibits superior adsorption capabilities compared to other adsorbents, with a high adsorption capacity of 2,199.971 mg/L.

3.6.2. Commercialization potential

Table 8 shows the commercial potential of TFMA as compared to commercial activated carbon. Since TFMA exhibited high adsorption capacity (2,199.971 mg/g) at 60°C within 30 min with as low as 1.24 USD/kg compared to commercial activated carbon of 20–22 USD/kg, hence, the utilization of face mask wastes into adsorbents had established a high commercial potential among the other non-renewable activated carbon.

4. Conclusion

This research work indicated that TFMA possessed excellent characteristics for MG adsorption. The TFMA was synthesized through thermal treatment at 800°C for 21 h. Both RFM and TFMA are mostly composed of alkane and alkene groups followed by carbonyl group and glucose

Table 7
Comparison of treated face mask adsorbent with other adsorbents

Source of adsorbents	Q_m (mg/g)	Types of dyes	References
Natural materials	124.9	Methylene blue	[26]
	649.37	Direct red 23	[26]
Clay minerals	14.9–16.5	Malachite green	[27]
Zeolites	20	Methylene blue	[28]
Bio-adsorbents			
Fungal	86.72–111.72	Reactive red 3	[29]
Bacterial	161.32	Malachite green	[30]
	183.44	Methylene blue	[30]
Algal	28.55	Methylene blue	[31]
Agricultural and industrial materials adsorbents			
Rice husk	373.02	Malachite green	[32]
Coffee husk	263	Malachite green	[33]
Oil palm empty agricultural waste bunch fiber	393.67	Cibacron blue	[34]
Almond shell	833.33	Methylene blue	[34]
Potato leaves	33.3	Malachite green	[35]
	52.6	Methylene blue	[35]
Potato stem	27	Malachite green	[35]
	41.6	Methylene blue	[35]
Plastic adsorbent			
PET bottle	743	Methylene blue	[36]
Real-world mixed waste plastics	769.2	Methylene blue	[37]
Polyvinyl chloride (PVC) plastic	240	Malachite green	[38]
Polyurethane (PU)	1,428	Malachite green	[39]
Polystyrene plastic (PS)	859.9	Methylene blue	[40]
Face mask wastes	2,199.971	Malachite green	Current research

Table 8
Comparison of treated face mask adsorbent with commercial activated carbon

	TFMA	Commercial activated carbon
Estimated production cost (USD/kg)	1.24 [4]	20–22 [41]
Maximum adsorption capacity (mg/g)	2,199.971	8.27 [42]
Raw material	Face mask wastes (no addition cost and readily available)	Coal (non-renewable)

ring based on C–C stretching, CH_3 rocking and C–H wagging vibration. As a result of the treatment process, the elevated temperatures caused the weakening and breaking of intermolecular bonds in C–C, C=C, and C–H, leading to variations in the presence of certain functional groups in TFMA. This phenomenon resulted in the formation of double bond functional groups like alkene and carbonyl groups. Moreover, the surface morphology analysis revealed that RFM exhibited a spherical porous carbon sorbent structure, which may facilitate the adsorption process. In contrast, the surface morphology of TFMA residues displayed a heterogeneous, flaky structure, indicating the successful implementation of the thermal treatment. Elemental analysis demonstrated that carbon was the predominant element in RFM, followed by oxygen and calcium. In contrast, TFMA was primarily composed of calcium and oxygen, with a limited amount of carbon. These findings provide evidence that the thermal treatment of RFM induced a change in the morphology of TFMA. Consequently, the significant presence of calcium-based components in TFMA facilitated the adsorption process, suggesting that the adsorption of MG onto TFMA can be considered a chemisorption process.

The adsorption capacity of TFMA was found to increase with an increase in contact time or initial dye concentration, as revealed by TFMA's behavior. The adsorption process was determined to be spontaneous, endothermic, and chemisorption in nature, with an increase in disorder at the solid-solution interface during the adsorption process. The analysis of adsorption isotherms and kinetics led to the identification of the BET isotherm and pseudo-

second-order kinetic models as the best-fit models, respectively, based on their high R^2 values close to 1 and low error function values. The isotherm results indicated that the adsorption of MG onto the heterogeneous surface of TFMA involved a multilayer process. Additionally, the kinetic model suggested the presence of a chemisorption process, supported by the high value of $\Delta H°$ in thermodynamics study. Consequently, it can be concluded that both physisorption and chemisorption may occur, with chemisorption predominantly taking place on the first layer and physisorption occurring in subsequent layers.

Acknowledgement

The authors thank University of Malaysia Perlis (UniMAP) and Faculty of Chemical Engineering & Technology for providing necessary facilities and support throughout the research.

References

[1] X.-G. Chen, S.-S. Lv, S.-T. Liu, P.-P. Zhang, A.-B. Zhang, J. Sun, Y. Ye, Adsorption of methylene blue by rice hull ash, Sep. Sci. Technol., 47 (2012) 147–156.
[2] S. Jung, S. Lee, X. Dou, E.E. Kwon, Valorization of disposable COVID-19 mask through the thermo-chemical process, Chem. Eng. J., 405 (2021) 126658, doi: 10.1016/j.cej.2020.126658.
[3] R. Kumar, B. Ruj, A.K. Sadhukhan, P. Gupta, Impact of fast and slow pyrolysis on the degradation of mixed plastic waste: product yield analysis and their characterization, J. Energy Inst., 92 (2019) 1647–1657.
[4] J. Serafin, J. Sreńscek-Nazzal, A. Kamińska, O. Paszkiewicz, B. Michalkiewicz, Management of surgical mask waste to activated carbons for CO_2 capture, J. CO_2 Util., 59 (2022) 101970, doi: 10.1016/j.jcou.2022.101970.
[5] I. Anastopoulos, I. Pashalidis, Single-use surgical face masks, as a potential source of microplastics: do they act as pollutant carriers?, J. Mol. Liq., 326 (2021) 115247, doi: 10.1016/j.molliq.2020.115247.
[6] A. Nasrullah, H. Khan, A.S. Khan, Z. Man, N. Muhammad, M.I. Khan, N.M. Abd El-Salam, Potential biosorbent derived from *Calligonum polygonoides* for removal of methylene blue dye from aqueous solution, Sci. World J., 2015 (2015) 562693, doi: 10.1155/2015/562693.
[7] J.A. Tantray, S. Mansoor, R.F.C. Wani, N.U. Nissa, Chapter 39 – Serial Dilution of the Bacterial Cells, in: Basic Life Science Methods, Academic Press, 2023, pp. 163–165.
[8] E. Marya Mistar, T. Alfatah, M. Dani Supardan, Synthesis and characterization of activated carbon from *Bambusa vulgaris striata* using two-step KOH activation, J. Mater. Res. Technol., 9 (2020) 6278–6286.
[9] M. Munoz, D. Ortiz, J. Nieto-Sandoval, Z.M. de Pedro, J.A. Casas, Adsorption of micropollutants onto realistic microplastics: role of microplastic nature, size, age, and NOM fouling, Chemosphere, 283 (2021) 131085, doi: 10.1016/j.chemosphere.2021.131085.
[10] C. Arora, P. Kumar, S. Soni, J. Mittal, A. Mittal, B. Singh, Efficient removal of malachite green dye from aqueous solution using *Curcuma caesia* based activated carbon, Desal. Water Treat., 195 (2020) 341–352.
[11] A.A. Ahmad, A.T.M. Din, N.K.E.M. Yahaya, A. Khasri, M.A. Ahmad, Adsorption of basic green 4 onto gasified *Glyricidia sepium* woodchip based activated carbon: optimization, characterization, batch and column study, Arabian J. Chem., 13 (2020) 6887–6903.
[12] T.A. Aragaw, Surgical face masks as a potential source for microplastic pollution in the COVID-19 scenario, Mar. Pollut. Bull., 159 (2020) 111517, doi: 10.1016/j.marpolbul.2020.111517.
[13] Z. Wang, C. An, X. Chen, K. Lee, B. Zhang, Q. Feng, Disposable masks release microplastics to the aqueous environment with exacerbation by natural weathering, J. Hazard. Mater., 417 (2021) 126036, doi: 10.1016/j.jhazmat.2021.126036.
[14] J.J. Hernández, M. Lapuerta, E. Monedero, Characterisation of residual char from biomass gasification: effect of the gasifier operating conditions, J. Cleaner Prod., 138 (2016) 83–93.
[15] P. Wang, W. Chen, R. Zhang, Y. Xing, Enhanced removal of malachite green using calcium-functionalized magnetic biochar, Int. J. Environ. Res. Public Health, 19 (2022) 3247, doi: 10.3390/ijerph19063247.
[16] S. Banerjee, G.C. Sharma, R.K. Gautam, M.C. Chattopadhyaya, S.N. Upadhyay, Y.C. Sharma, Removal of malachite green, a hazardous dye from aqueous solutions using *Avena sativa* (oat) hull as a potential adsorbent, J. Mol. Liq., 213 (2016) 162–172.
[17] H. Nuradibah, S.Y. Chin, H. Anwaruddin, Study of important operating parameters for the adsorption of acrylic acid from wastewater using palm ash, J. Appl. Sci., 14 (2014) 1385–1390.
[18] N.N. Ahmad, A.A. Ahmad, A. Khasri, Effective removal of methylene blue from aqueous solution by adsorptioonto gasification char: isotherm, kinetic and thermodynamics studies, Desal. Water Treat., 285 (2023) 264–273.
[19] A.A. Ahmad, A.T.M. Din, N.K.E.M. Yahaya, J. Karim, M.A. Ahmad, Atenolol sequestration using activated carbon derived from gasified *Glyricidia sepium*, Arabian J. Chem., 13 (2020) 7544–7557.
[20] N.A.H. Ab Aziz, U.F. Md Ali, A.A. Ahmad, M.I.H. Mohamed Dzahir, M.H. Khamidun, M.F. Abdullah, Non-functionalized oil palm waste-derived reduced graphene oxide for methylene blue removal: isotherm, kinetics, thermodynamics, and mass transfer mechanism, Arabian J. Chem., 16 (2023) 104387, doi: 10.1016/j.arabjc.2022.104387.
[21] A.A. Ahmad, M.A. Ahmad, U.F. Md Ali, K. Khoo, Gasification char residues management: assessing the characteristics for adsorption application, Arabian J. Chem., 16 (2023) 104993, doi: 10.1016/j.arabjc.2023.104993.
[22] S. Banerjee, M.C. Chattopadhyaya, Adsorption characteristics for the removal of a toxic dye, tartrazine from aqueous solutions by a low cost agricultural by-product, Arabian J. Chem., 10 (2017) S1629–S1638.
[23] K.M. Doke, E.M. Khan, Equilibrium, kinetic and diffusion mechanism of Cr(VI) adsorption onto activated carbon derived from wood apple shell, Arabian J. Chem., 10 (2017) S252–S260.
[24] S. Kwon, M. Fan, H.F.M. DaCosta, A.G. Russell, K.A. Berchtold, M.K. Dubey, CO_2 Sorption, D.A. Bell, B.F. Towler, M. Fan, Eds., Coal Gasification and Its Applications, Elsevier, Boston, 2011, pp. 293–339.
[25] Y.T. Gebreslassie, Equilibrium, kinetics, and thermodynamic studies of malachite green adsorption onto fig (*Ficus cartia*) leaves, J. Anal. Methods Chem., 2020 (2020) 7384675, doi: 10.1155/2020/7384675.
[26] F. Largo, R. Haounati, S. Akhouairi, H. Ouachtak, R. El Haouti, A. El Guerdaoui, N. Hafid, D.M.F. Santos, F. Akbal, A. Kuleyin, A. Jada, A.A. Addi, Adsorptive removal of both cationic and anionic dyes by using sepiolite clay mineral as adsorbent: experimental and molecular dynamic simulation studies, J. Mol. Liq., 318 (2020) 114247, doi: 10.1016/j.molliq.2020.114247.
[27] R. Han, Y. Wang, Q. Sun, L. Wang, J. Song, X. He, C. Dou, Malachite green adsorption onto natural zeolite and reuse by microwave irradiation, J. Hazard. Mater., 175 (2010) 1056–1061.
[28] H.F. Youssef, R.A. Nasr, E.A. Abou El-Anwar, H.S. Mekky, S.H. Abd El Rahim, Preparation and characterization of different zeolites from andesite rock: product evaluation for efficient dye removal, Microporous Mesoporous Mater., 328 (2021) 111485, doi: 10.1016/j.micromeso.2021.111485.
[29] V. Karthik, P.S. Kumar, K. Harsha Vardhan, K. Saravanan, N. Nithyakala, Adsorptive behaviour of surface tailored fungal biomass for the elimination of toxic dye from wastewater, Int. J. Environ. Anal. Chem., 102 (2020) 4710–4725.
[30] Y. Zhang, C. Hui, R. Wei, Y. Jiang, L. Xu, Y. Zhao, L. Du, H. Jiang, Study on anionic and cationic dye adsorption behavior and mechanism of biofilm produced by *Bacillus amyloliquefaciens*

DT, Appl. Surf. Sci., 573 (2022) 151627, doi: 10.1016/j.apsusc.2021.151627.
[31] R. Foroutan, R. Mohammadi, J. Razeghi, B. Ramavandi, Performance of algal activated carbon/Fe_3O_4 magnetic composite for cationic dyes removal from aqueous solutions, Algal Res., 40 (2019) 101509, doi: 10.1016/j.algal.2019.101509.
[32] C.Y. Tsai, P.Y. Lin, S.L. Hsieh, R. Kirankumar, A.K. Patel, R.R. Singhania, C. Di Dong, C.W. Chen, S. Hsieh, Engineered mesoporous biochar derived from rice husk for efficient removal of malachite green from wastewaters, Bioresour. Technol., 347 (2022) 126749, doi: 10.1016/j.biortech.2022.126749.
[33] T.P. Krishna Murthy, B.S. Gowrishankar, M.N. Chandra Prabha, M. Kruthi, R. Hari Krishna, Studies on batch adsorptive removal of malachite green from synthetic wastewater using acid treated coffee husk: equilibrium, kinetics and thermodynamic studies, Microchem. J., 146 (2019) 192–201.
[34] J. Oliver Paul Nayagam, K. Prasanna, Utilization of shell-based agricultural waste adsorbents for removing dyes: a review, Chemosphere, 291 (2022) 132737, doi: 10.1016/j.chemosphere.2021.132737.
[35] N. Gupta, A.K. Kushwaha, M.C. Chattopadhyaya, Application of potato (*Solanum tuberosum*) plant wastes for the removal of methylene blue and malachite green dye from aqueous solution, Arabian J. Chem., 9 (2016) S707–S716.
[36] N.A. El Essawy, S.M. Ali, H.A. Farag, A.H. Konsowa, M. Elnouby, H.A. Hamad, Green synthesis of graphene from recycled PET bottle wastes for use in the adsorption of dyes in aqueous solution, Ecotoxicol. Environ. Saf., 145 (2017) 57–68.
[37] J. Gong, J. Liu, X. Chen, Z. Jiang, X. Wen, E. Mijowska, T. Tang, Converting real-world mixed waste plastics into porous carbon nanosheets with excellent performance in the adsorption of an organic dye from wastewater, J. Mater. Chem. A, 3 (2015) 341–351.
[38] F. Lian, B. Xing, L. Zhu, Comparative study on composition, structure, and adsorption behavior of activated carbons derived from different synthetic waste polymers, J. Colloid Interface Sci., 360 (2011) 725–730.
[39] Z. Li, K. Chen, Z. Chen, W. Li, B.W. Biney, A. Guo, D. Liu, Removal of malachite green dye from aqueous solution by adsorbents derived from polyurethane plastic waste, J. Environ. Chem. Eng., 9 (2021) 104704, doi: 10.1016/j.jece.2020.104704.
[40] W. Li, Z. Xie, S. Xue, H. Ye, M. Liu, W. Shi, Y. Liu, Studies on the adsorption of dyes, Methylene blue, Safranin T, and Malachite green onto Polystyrene foam, Sep. Purif. Technol., 276 (2021) 119435, doi: 10.1016/j.seppur.2021.119435.
[41] E. Menya, P.W. Olupot, H. Storz, M. Lubwama, Y. Kiros, Production and performance of activated carbon from rice husks for removal of natural organic matter from water: a review, Chem. Eng. Res. Des., 129 (2018) 271–296.
[42] I.D. Mall, V.C. Srivastava, N.K. Agarwal, I.M. Mishra, Adsorptive removal of malachite green dye from aqueous solution by bagasse fly ash and activated carbon-kinetic study and equilibrium isotherm analyses, Colloids Surf., A, 264 (2005) 17–28.